Thermalization in the one-dimensional Salerno model lattice

Thudiyangal Mithun,[1] Aleksandra Maluckov [●],[2,3] Bertin Many Manda [●],[4] Charalampos Skokos [●],[4] Alan Bishop,[5]
Avadh Saxena [●],[5] Avinash Khare,[6] and Panayotis G. Kevrekidis [●][1]

[1]*Department of Mathematics and Statistics, University of Massachusetts, Amherst, Massachusetts 01003-4515, USA*

[2]*Vinca Institute of Nuclear Sciences, University of Belgrade, National Institute of the Republic of Serbia, P.O.B. 522, 11001 Belgrade, Serbia*

[3]*Center for Theoretical Physics of Complex Systems, Institute for Basic Science, Daejeon 34051, S. Korea*

[4]*Nonlinear Dynamics and Chaos Group, Department of Mathematics and Applied Mathematics, University of Cape Town, Rondebosch,
7701 Cape Town, South Africa*

[5]*Center for Nonlinear Studies and Theoretical Division, Los Alamos National Laboratory, Los Alamos, New Mexico 87545, USA*

[6]*Department of Physics, Savitribai Phule Pune University, Pune 411007, India*

The Salerno model constitutes an intriguing interpolation between the integrable Ablowitz-Ladik (AL) model and the more standard (nonintegrable) discrete nonlinear Schrödinger (DNLS) one. The competition of local on-site nonlinearity and nonlinear dispersion governs the thermalization of this model. Here, we investigate the statistical mechanics of the Salerno one-dimensional lattice model in the nonintegrable case and illustrate the thermalization in the Gibbs regime. As the parameter interpolating between the two limits (from DNLS toward AL) is varied, the region in the space of initial energy and norm densities leading to thermalization expands. The thermalization in the non-Gibbs regime heavily depends on the finite system size; we explore this feature via direct numerical computations for different parametric regimes.

I. INTRODUCTION

Enlightening of the thermalization properties of lattice dynamical models and complex networks is a crucial issue in understanding and exploiting the transport and localization phenomena of relevance to a wide range of physical problems. In spite of substantial research, the coexistence of diverse physical processes and correlations among them developing on different space-time scales lacks a conclusive interpretation [1–11]. It is therefore natural to expect that the application of statistical and thermodynamical approaches and related mixing, ergodicity, and energy equipartition concepts to such problems is a topic of substantial ongoing interest. Among the numerous prototypical nonlinear physical examples are the statistics of the Fermi-Pasta-Ulam-Tsingou chains [11,12], chains of Josephson junctions [13], Gross-Pitaevskii or discrete nonlinear Schrödinger lattices with different types of nonlinearities [14–20], Toda and Morse lattices [21], etc. The localized wave patterns that naturally emerge in such systems as a result of the interplay between lattice dispersion and nonlinearity play a crucial role in the thermalization and lattice dynamics [22,23].

Our study is partially motivated by recent findings regarding the statistics of different discrete nonlinear physical systems [13,20] in which, as a core mechanism, the relaxation of nonlinear localized excitations and related ergodization is considered. In the many-body systems, the ergodization demands infinite-time averages of an observable during a microcanonical evolution to match with their proper phase space averages.

In a class of dynamical systems where ergodization timescales sensitively depend on the control parameters, dynamical glass behavior is postulated to be a generic system property on the route toward the integrable limits [13]. This glassy behavior is further attributed to the short-range network in the action space. Hence it is interesting to explore the thermalization in a system where both an integrable and a nonintegrable (yet physically relevant) limit can exist as a suitable parameter is varied. One such model is the Salerno model (SM) [24]. Despite the two decades that have ensued since the attempt to thermodynamically describe the discrete nonlinear Schrödinger (DNLS) model [25,26], the problem continues to attract significant attention; see Refs. [27–29] for recent studies. On the other hand, the SM has provided an excellent platform for exploring the interplay between nonlinear localized structures and near-linear extended ones, between nonlinearity and dispersion, on the path between integrability and nonintegrability; see, e.g., [30] for a recent review.

Bearing the above features in mind, our aim here is to explore the statistical mechanics and thermalization properties of the Salerno model. In addition to interpolating between the fully integrable Ablowitz-Ladik (AL) and the DNLS models [6,24,31–33], the SM incorporates coexistence and competition of nonlinear dispersion and nonlinear local interactions. In the present work, we adopt a grand-canonical description of SM, decomposing the parameter space of energy and norm densities (corresponding to the conserved quantities of the energy and total norm, respectively) into Gibbs and non-Gibbs regimes. In the former, we expect "regular" thermalization. In the latter non-Gibbs regime, we expect to encounter energy localization in the form of long-living nonlinear excitations in line with the corresponding DNLS prediction of [25]. One part of the intriguing story is that as the SM parameters

are varied linearly interpolating between the DNLS and the AL models, we should be able to observe that regions that used to belong in the non-Gibbs regime will now "regularly" thermalize as we approach the AL limit. That is, we should be able to observe a key change in behavior along the paths of parametric variation considered. However, there are also additional features that add to the complexity of the story.

While the general expectation previously was that the non-Gibbs regime is nonergodic, a recent study of the DNLS lattice using the statistics of excursion times of equilibrium Poincaré manifolds and finite-time average distributions of an observable has shown that a part of the non-Gibbs regime is weakly ergodic [11,13,20] in the setting of finite lattices. The nonergodicity may be a feature of the thermodynamic limit of infinite lattices. Motivated by this array of recent developments and challenging observations, we numerically investigate the thermalization in the SM with respect to both the Gibbs and non-Gibbs regimes. We will utilize a combination of thermodynamic tools, including the transfer integral approach, and direct numerical simulations, and measures of both statistical properties [e.g., the probability distribution function (PDF) of different amplitudes] and dynamical properties (such as Lyapunov exponents) in order to characterize the system, including for different lattice sizes, so as to address the fundamental question of the behavior of the SM under parametric, initial condition and lattice size variations.

Among the motivating factors for considering the present model, we cite the following. First, the integrable limit of the SM (i.e., the Ablowitz-Ladik lattice) is well known and in this integrable limit there exists a systematic procedure to build the associated conservation laws. As a result, our model provides a particularly relevant platform for exploring the connection between statistical mechanics and integrability and conservation laws. Second, in our study, we will see that it will be possible to control the nonlinear dispersion parameter. This will induce a network in the action space that is different from the case of the standard DNLS model due to the long range of the network. This long-range network will considerably affect the lifetime of excitations observed in the system. Finally, the model enables a monoparametric flexibility that allows control of the transition between Gibbs and non-Gibbs regimes for the same point in the thermodynamic (energy-norm) space under consideration. We find that these intriguing features of the SM distinguish it from earlier studies and render it a particularly suitable test bed for further considerations in this direction.

Our presentation is structured as follows. In Sec. II, we present the fundamentals of the model. In Sec. III, we lay the theoretical foundations for the statistical mechanical analysis of the SM. In Sec. IV, we present the corresponding numerical analysis (both through statistical and dynamical diagnostics), and finally in Sec. V we summarize our findings, and present our conclusions, as well as some directions of future research. The appendices present details of our theoretical analysis and results for the model's Lyapunov exponent.

II. MODEL DESCRIPTION

The SM can be considered as a discretization of the continuous fully integrable cubic nonlinear Schrödinger equation.

Its equations of motion [24,33], upon suitable rescaling of the intersite coupling, read

$$i\frac{d\psi_n}{dt} = (\psi_{n+1} - 2\psi_n + \psi_{n-1})$$
$$+ (\mu|\psi_n|^2)(\psi_{n+1} + \psi_{n-1}) + \gamma|\psi_n|^2\psi_n, \quad (1)$$

where ψ_n is the complex wave function at site n, $\gamma = 2(1 - \mu)$, and $\mu \geqslant 0$. The parameter γ represents the strength of local nonlinear interaction and μ represents the strength of nonlinear dispersion (intersite nonlinearity). In the limit $\mu \to 0$ the model reduces to the standard DNLS equation with on-site (local) cubic nonlinearity. On the contrary, the limit $\gamma = 0$ corresponds to the completely integrable AL model [26,34,35]. A simple transformation $\psi_n \to \psi_n e^{i2t}$ leads to

$$i\frac{d\psi_n}{dt} = (1 + \mu|\psi_n|^2)(\psi_{n+1} + \psi_{n-1}) + \gamma|\psi_n|^2\psi_n. \quad (2)$$

The full set of invariants of motion in the completely integrable, AL limit is considered in [36], while the nonintegrable DNLS limit is characterized by two integrals of motion. Therefore, regardless of the limits, Eq. (2) can be characterized by two conserved quantities: norm $\mathcal{A}$ and Hamiltonian $\mathcal{H}$ [37]:

$$\mathcal{A} = \sum_{n=1}^{N} \mathcal{A}_n, \quad \mathcal{A}_n = \frac{1}{\mu}\ln|1 + \mu|\psi_n|^2|,$$

$$\mathcal{H} = \sum_{n=1}^{N}\left[-\frac{\gamma}{\mu}\mathcal{A}_n + \psi_n\psi_{n+1}^* + \psi_n^*\psi_{n+1} + \frac{\gamma}{\mu}|\psi_n|^2\right], \quad (3)$$

where N is the total number of lattice nodes and periodic boundary conditions are used.

The SM equations [Eqs. (2)] can be derived from the Hamiltonian $\mathcal{H}$

$$\frac{d\psi_n}{dt} = \{\mathcal{H}, \psi_n\}, \quad (4)$$

with respect to the canonically conjugated pairs of variables ψ_n and $i\psi_n^*$ defining the deformed Poisson brackets [38]

$$\{\psi_n, \psi_m^*\} = i(1 + \mu|\psi_n|^2)\delta_{nm}, \quad \{\psi_n, \psi_m\} = \{\psi_n^*, \psi_m^*\} = 0. \quad (5)$$

III. STATISTICAL MECHANICS OF THE SALERNO NETWORK

Here we attempt to clarify the thermalization properties of the SM starting from the DNLS limit $\mu = 0$, in which the thermalization and statistical properties are extensively investigated [2,20,25,38,39]. After a brief remark on findings in the DNLS limit we probe the extension of the Gibbs approach to the SM with competing local and nonlocal nonlinearities.

Applying the canonical transformation $\psi_n = \sqrt{A_n}\exp(i\phi_n)$, where A_n and ϕ_n denote the amplitude and phase, we obtain from Eq. (3) the following expressions

for the conserved quantities:

$$\mathcal{A} = \frac{1}{\mu} \sum_{n=1}^{N} \ln|1 + \mu A_n|,$$

$$\mathcal{H} = \sum_{n=1}^{N} \left[-\frac{\gamma}{\mu^2} \ln|1 + \mu A_n| + \frac{\gamma}{\mu} A_n \right.$$
$$\left. + \sqrt{A_n A_{n+1}} \cos(\phi_n - \phi_{n+1}) \right]. \quad (6)$$

The corresponding grand-canonical partition function of the SM can then be presented in a form

$$Z = \int_0^\infty \int_0^{2\pi} \prod_{n=1}^{N} d\phi_n dA_n e^{-\beta(\mathcal{H} + \alpha \mathcal{A})}, \quad (7)$$

where parameters α and β are introduced in analogy with the chemical potential and the inverse temperature [25] (i.e., they are the corresponding Lagrange multipliers). This expression can be reduced to the integral form after the integration over the phase variables ϕ_n:

$$Z = (2\pi)^N \int_0^\infty \prod_{n=1}^{N} dA_n$$
$$\times I_0(2\beta\sqrt{A_n A_{n+1}}) e^{-\beta \sum_n [(-\frac{\gamma}{\mu^2} + \frac{\alpha}{\mu}) \ln|1 + \mu A_n| + \frac{\gamma}{\mu} A_n]}, \quad (8)$$

where I_0 stands for the modified Bessel function of the first kind (with index 0).

In the thermodynamic limit of large systems $N \to \infty$, the integral can be evaluated exactly using the eigenfunctions and eigenvalues of the transfer integral operator (TIO) (Appendix A). From the latter calculation, in the infinite-temperature limit $\beta \to 0$, the following relation between the energy ($h = \mathcal{H}/N$) and norm ($a = \mathcal{A}/N$) density can be derived,

$$h = \frac{2(1-\mu)a^2}{(1-a\mu)}, \quad (9)$$

which for $\mu = 0$ reduces to the corresponding relation of the DNLS lattice [6,20,25]. In terms of the largest eigenvalue λ_0 of the kernel of Eq. (A10), the norm density a can be expressed as $a = \int_0^\infty y_0^2(A) A \, dA$, where $y_0^2(A)$ represents the probability distribution of amplitudes $P(A)$ corresponding to the largest eigenvalue.

Following the statistical mechanical analysis of Appendix A, we distinguish the Gibbs regime in the (a, h) parameter space by determining the characteristic phase curves $\beta \to \infty$ and $\beta \to 0$. While formally the first one separates the microcanonically inaccessible regime from the Gibbs region of phase space, the second one separates regions characterized by positive temperature ($\frac{1}{\beta} > 0$) from those with negative temperature ($\frac{1}{\beta} < 0$) whose accessibility is experimentally and numerically proven and which leads to the prolonged emergence of coherent structures.

The transition curve $\beta \to \infty$ can be determined from

$$h = -\frac{\gamma}{\mu} a + \frac{\gamma}{\mu^2}(e^{\mu a} - 1) - \frac{2}{\mu}(e^{\mu a} - 1), \quad \text{and}$$
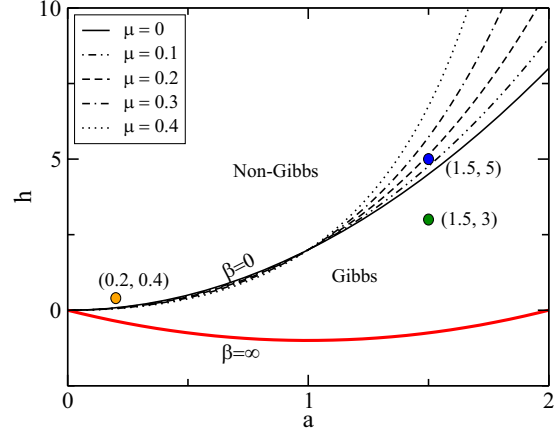
$$a = \frac{1}{\mu} \ln(1 + \mu d), \quad (10)$$

FIG. 1. The norm and energy density parameter space (a, h) of the SM. The area between the curves $\beta = 0$ (black thin lines) and $\beta \to \infty$ (red solid thick line) in the parameter space (a, h) denotes the Gibbs regime of anticipated thermalization [Eq. (7) is valid] for a few values of the parameter μ (=0, 0.1, 0.2, 0.3, 0.4) respectively represented by solid, dot-dot-dashed, dashed, dot-dashed, and dotted black curves. The area above $\beta = 0$ will be referred to as non-Gibbs, where Eq. (7) is invalid. The region below $\beta \to \infty$ is forbidden for any microcanonical states. The green, blue, and orange symbols respectively represent $(a = 1.5, h = 3)$, $(a = 1.5, h = 5)$, and $(a = 0.2, h = 0.4)$.

by minimizing the Hamiltonian Eq. (3) with the plane-wave solution in a form $\psi_n = \sqrt{d} e^{in\theta}$ and taking $\theta = \pi$.

To clarify the thermalization properties, we calculate the amplitude probability density function $[P(A)]$ and the excursion time probability (P_+). The $P(A)$ obtained from a direct numerical simulation of Eq. (1) is compared with the one calculated via the TIO approach [25]. On the other hand, the time intervals which the local norms spend between two consecutive intersections of the plane $A_n = a$ (the Poincaré section) form the excursion time distribution $P_+(\tau)$, where $+$ denotes $A_n > a$ and $\tau_n(i) = t_n^{i+1} - t_n^i$. The distribution has the average μ_τ and the standard deviation σ_τ. The value of σ_τ can be associated with the divergence of the average excursion time and weak nonergodicity in the lattice [11,20]. A third measure of thermalization is the finite-time average (FTA) of the observable,

$$A_{n,T} = \frac{1}{T} \int_0^T A_n(t) \, dt. \quad (11)$$

The distribution of the FTA for a set of trajectories is characterized by the first moment $m_1(T)$ and the second moment $m_2(T)$. For an ergodic regime, at large time $m_2(T \to \infty) \to 0$ [13,40].

In order to investigate thermalization in the SM we perform numerical experiments and base our corresponding analysis on the system's phase diagram illustrated in Fig. 1, in the parameter space (a, h). The red curve corresponds to the zero-temperature limit $\beta \to \infty$, while black curves correspond to the infinite-temperature limit, $\beta \to 0$ for a few values of parameter μ in the interval 0 to 0.5. These are based on the analytical predictions of these limits given above (and derived in the Appendix A). The region between $\beta = \infty$ and $\beta = 0$

lines denotes the Gibbs regime of the SM where the approach based on the grand-canonical-Gibbs statistics (Eq. (7) is applicable [20,25]) and thus the model is expected to thermalize. Outside this region, a non-Gibbs regime featuring the presence of coherent structures is identified where, however, for finite domains only weak nonergodicity may be present as discussed in [20]. We now proceed to analyze our numerical computations at different selected points within this parameter space bearing in mind that a key feature of the SM case is that regimes identified as non-Gibbsian for the DNLS model of $\mu = 0$ can be Gibbsian for larger values of μ.

IV. NUMERICAL ANALYSIS

In this section, we describe the numerically obtained results for various μ values corresponding to both the Gibbs and non-Gibbs regimes. This section aims to explore the thermalization properties in these regimes induced by the competing nonlinearities, local nonlinear interaction, and nonlinear hopping, which cause self-trapping and nonlinear dispersion, respectively.

We solve Eq. (1) numerically by using an explicit Runge-Kutta algorithm of order 8, called DOP853 [41–43]. We set the relative energy error $|\frac{\mathcal{H}(t)-\mathcal{H}(0)}{\mathcal{H}(0)}|$ and norm $|\frac{\mathcal{A}(t)-\mathcal{A}(0)}{\mathcal{A}(0)}|$ error threshold to 10^{-4}. Initially a small complex random perturbation is added to the plane waves

$$\psi_n(0) = \sqrt{d}\,\exp{(i\phi_n)},$$

where $d = \mu^{-1}[\exp(a\mu) - 1] = \mathcal{A}/N$. Unless otherwise mentioned we use a total integration time of $T = 10^7$ and a system size of $N = 256$. As an additional dynamical diagnostic of the degree of chaos in the system, we discuss the use of the finite-time maximal Lyapunov characteristic exponent (mLCE) in Appendix B.

A. Gibbs regime

We consider the parameter set ($a = 1.5$, $h = 3$) which is in the Gibbs regime irrespective of the μ value considered (see Fig. 1). The numerically calculated PDFs, $P(A)$ (solid curves in Fig. 2), show that the amplitude A increases with the increase of μ. In order to ensure that the obtained $P(A)$ represent a thermalized state, we compare them with the probability distributions obtained by the TIO approach based on the corresponding dominant (squared) eigenvector of the TIO approach (see, e.g., Appendix A and also [25]). Our results indicate that TIO solutions (dashed curves in Fig. 2) and numerical results match very well, which corroborates the anticipated thermalization in this regime.

The amplitude profiles corresponding to the case ($a = 1.5$, $h = 3$) for three different μ values are shown in Fig. 3. Though high-amplitude nonlinear localized excitations emerge in the system as a result of the modulational instability of the initial condition, they are all rather short lived and the long-time evolution of the system appears to be thermalized into a phononic bath and without evidence of any kind of persistent localization. The thermalization is further verified from the second moment, $m_2(T)$, of the FTA of local integral norms (Fig. 4), which decays as $1/T$ at large times for all values of the considered μ.
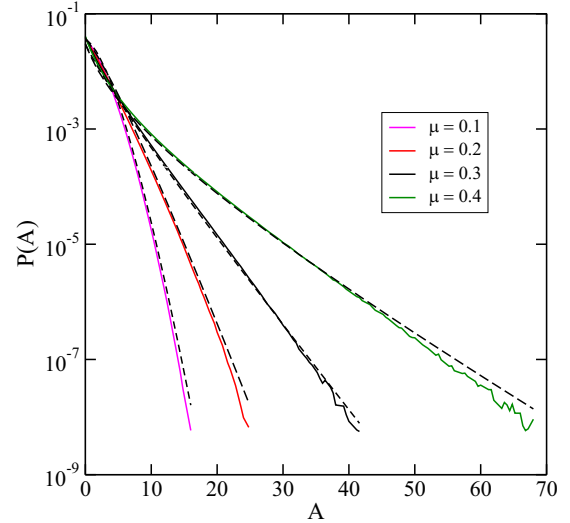

FIG. 2. The PDF of local norms (amplitudes) $A_n = |\psi_n|^2$ for different values of μ for the parameter set ($a = 1.5$, $h = 3$). Dashed curves represent the results obtained analytically by the TIO method, while solid curves show the numerically generated PDFs. The total integration time is $T = 10^7$. TIO curves nicely fit to numerical ones in the Gibbs regime.

Additionally, the calculation of the mLCE Λ in Appendix B shows that $\Lambda > 0$ (red squares in Fig. 10) which is a signature of chaoticity in the system.

B. Non-Gibbs regime

To investigate the thermalization in the non-Gibbs regime, we consider the parameter set ($a = 1.5$, $h = 5$), the blue colored point in Fig. 1. For this parameter set, the critical value $\mu_c \approx 0.17$ sets the transition point from the Gibbs to the non-Gibbs regime. That is, for $\mu > \mu_c$, ($a = 1.5$, $h = 5$) is in the Gibbs regime, where TIO solutions match exactly with the numerically calculated $P(A)$ as shown in Fig. 5.

For $\mu < \mu_c$, the tail of $P(A)$ develops a bump (at suitably large amplitudes) at initial times, which can be associated with the accumulation of large-amplitude nonlinear excitations. In spite of it, we observed an exponential cutoff that might be related to the finite size of the system, which has been shown to affect all statistical measures we calculated in the non-Gibbs regime. It is worthwhile to observe that this bump is no longer present in the cases of $\mu > \mu_c$ (while the cutoff is still featured) and at large times for $\mu < \mu_c$. To corroborate this observation in the system, but also to explore the role of the finite-size effects, we first plot the amplitude profiles as a function of time for three different values of μ, Fig. 6. Interestingly, for all values of μ, both those that belong to the Gibbs regime [$\mu = 0.5$ and $\mu = 0.2$ of panels (c) and (b); the latter is near and above the critical value] and even in the non-Gibbs regime ($\mu = 0.05$), the decay of initially generated large-amplitude structures is eventually observed. Nevertheless, the coherent structures are significantly more prominent in the non-Gibbs case. The latter case of panel (a) represents the possibility of a non-Gibbsian regime which, however, within a finite lattice manifests the features of quasiergodic behavior as has been discussed in [20].
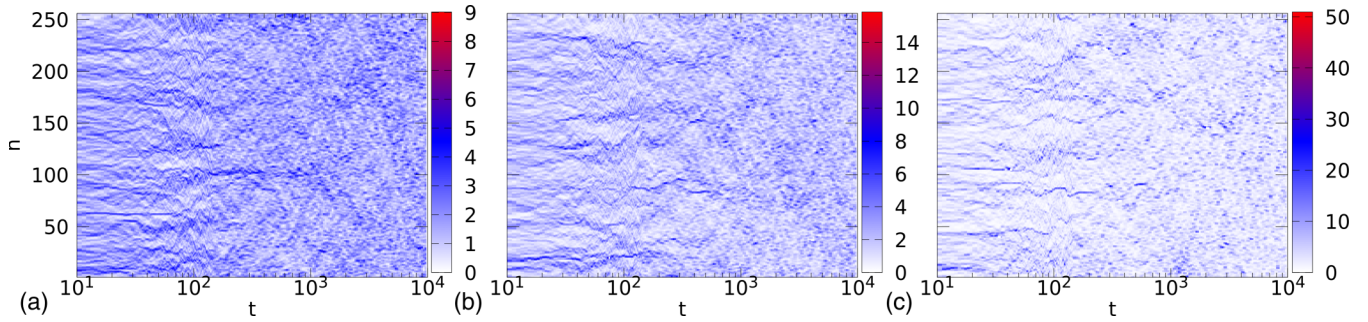
FIG. 3. The amplitude profiles in space (n)-time (t) in the Gibbs regime for three different μ values (a) $\mu = 0.05$, (b) $\mu = 0.2$, and (c) $\mu = 0.5$ at $(a = 1.5, h = 3)$ for the system size $N = 256$.

The second moment of the FTA of the integral local norms, shown in Fig. 7, decays over time for the considered μ values. The curves, however, do not indicate any distinctive behavior that differentiates the dynamics in Gibbs ($\mu > \mu_c$) and non-Gibbs regimes ($\mu < \mu_c$).

In line with recent developments in the field [13,20], it is quite relevant to explore the effects of the finite size of our computation and their implications in connection with the infinite domain thermodynamic analysis, e.g., implicit in the TIO calculations. To explore the role of finite system size, we calculate the variance, σ_τ^2, of the excursion time distribution for different system sizes as depicted in Fig. 8. Upon increasing the system size N, the variance σ_τ^2 increases indicating the significance of the finite-size effect in the thermalization of the non-Gibbs regime for $h \to h_{\beta=0}$. The somewhat nonsmooth nature of the growth might be related to the small number of initial conditions used for the averaging. Nevertheless, it can be conjectured that in the limit $N \to \infty$ the excitations in the non-Gibbs regime will be persistent. It is also worthwhile to note that in the calculation of the variance, σ_τ^2, the excitations whose lifetime is higher than the total integration time, $T = 10^7$, are not considered. On the other hand, the decay of the second moment, m_2, of the FTA distribution shown in Fig. 7 indicates that there are no such long-living excitations. Since we observed that the finite size plays a crucial role in the
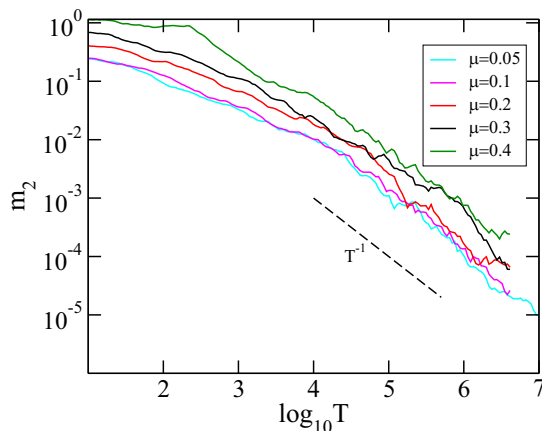
non-Gibbs regime for $h \to h_{\beta=0}$, we next consider a point in the parameter space (a, h), that is far from $h_{\beta=0}$. This higher ratio of $\frac{h}{h_{\beta=0}}$ can be more straightforwardly obtained for a small norm and we fix $(a = 0.2, h = 0.4)$ (orange symbol in Fig. 1). As the ratio $\frac{h}{h_{\beta=0}}$ becomes larger, the contribution of the nonlinear interaction term in Eq. (3) is higher due to the boundedness of the kinetic energy [25]. The corresponding amplitude evolutions are shown in Fig. 9 for three different values of μ. For all these μ values, the parameter set $(a = 0.2, h = 0.4)$ is in the non-Gibbs regime and accordingly, the amplitude evolution shows the presence of at least one excitation with lifetime greater than the total computation time. This hints at a nonergodic behavior for the considered long but finite time.

In summary, our analysis has illustrated that the Gibbs regime for the DNLS model remains Gibbsian for the SM
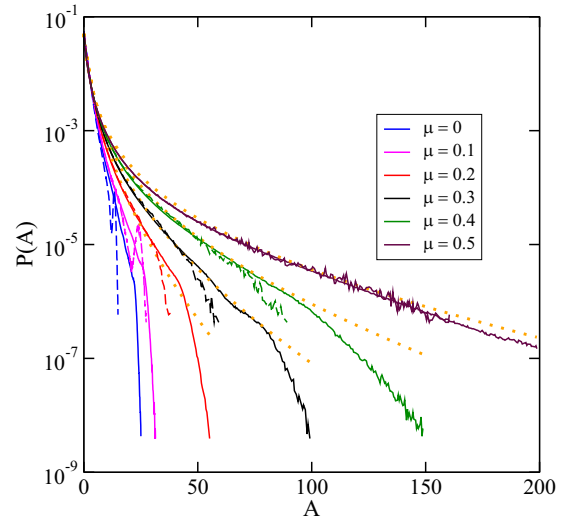

FIG. 4. The evolution of the second moment [$m_2(T)$] of FTA distributions of the integral local norms for the different values of μ corresponds to $(a = 1.5, h = 3)$. The dashed line represents $m_2 \propto T^{-1}$.

FIG. 5. The PDF of local norms (amplitudes) $A_n = |\psi_n|^2$ for different values of μ for the parameter set $(a = 1.5, h = 5)$. This arrangement is in the Gibbs regime for $\mu > 0.17$ and otherwise in the non-Gibbs regime. Different curves are associated with $\mu = 0, 0.1, 0.2, 0.3, 0.4, 0.5$ as shown in the legend. Dotted orange curves represent the results obtained analytically by the TIO method, while dashed and solid lines show the numerically generated $P(A)$ at two different times $T = 10^5$ and $T = 10^7$, respectively. TIO curves fit the numerical ones in the Gibbs regime, except for the large-amplitude tail region.
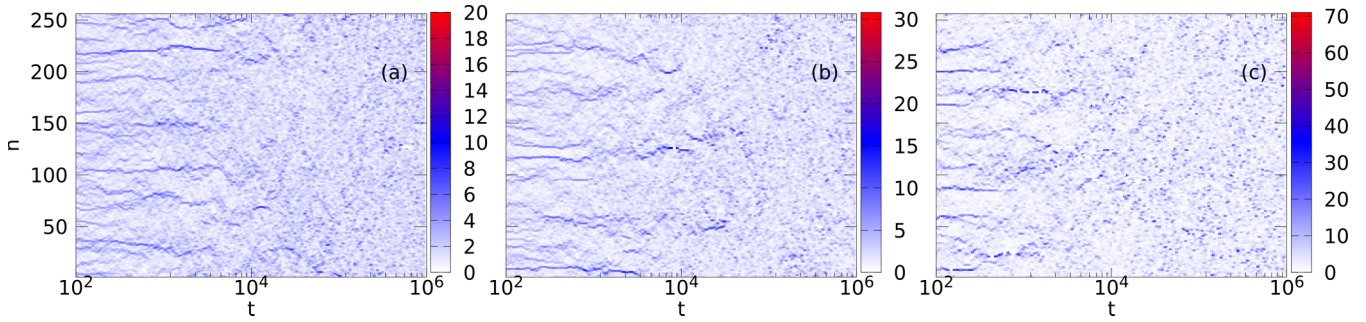
FIG. 6. In panels (a), (b), and (c), the amplitude profiles are respectively shown in the non-Gibbs regime ($\mu = 0.05$), near the critical point ($\mu = 0.2$), and in the Gibbs regime ($\mu = 0.5$) for $a = 1.5$, $h = 5$, and $N = 256$. In the non-Gibbs phase [panel (a)], the appearance of localized breathing structures is significantly more prominent than in the Gibbs regime [panel (c)].

of the present considerations in line with the corresponding analytical results. The situation becomes considerably more interesting beyond the thermalization limit of $\beta = 0$ for the DNLS; progressively the thermalization region of the (a, h) space expands upon increase of μ rendering nonthermalized parameter ranges for smaller μ thermalized as μ grows past a certain threshold. However, there exist additional features to consider. On the one hand, the finiteness of the lattice plays a considerable role as to whether nonergodicity will be preserved and it is indeed found that finite lattices may lead to an apparent ergodization. Nevertheless, as the domain size grows to infinity, so does the lifetime of the high-amplitude, nonlinear excitations in line with the thermodynamic model prediction. On the other hand, the thermalization in the non-Gibbs regime heavily depends on the $\frac{h}{h_{\beta=0}}$ ratio. When the latter becomes larger, then the system may find itself in a nonergodic regime even in the case of the finite-lattice (long-time) computations. These features are qualitatively reported here and merit additional quantification through extensive and highly demanding (in their computation time and accuracy) computations. Nevertheless, we believe that the above results offer useful insights in this direction. Further, the occurrence and dynamics of long-lived excitations in the system has been associated with the thermodynamics of the DNA double strand and its denaturation; such thermodynamic discussions

in a variety of Klein-Gordon models can be found in [44]. The family of models presented herein corresponds to the envelope dynamics of such Klein-Gordon settings.

V. CONCLUSIONS AND FUTURE CHALLENGES

The thermalization in the nonintegrable regime of the Salerno model (SM) has been investigated by using a combination of analytical and numerical techniques. More specifically, we have complemented the transfer integral operator (TIO) analysis by performing relevant long-time numerical simulations. In the latter, we have used a set of diagnostics such as the probability distribution of amplitudes and finite-time averages of local probability density (and its moments) as well as, e.g., Lyapunov characteristic exponents. A key feature of the model is the coexistence of local non-linearity and nonlinear dispersion. The competition between these two effects sets two limits, a nonintegrable and an integrable one, in the system, namely the discrete nonlinear Schrödinger (DNLS) and the Ablowitz-Ladik (AL) models. One can then monoparametrically interpolate between these limits. Our study has mainly focused on the nonintegrable limit, but provides a sense of the qualitative variation of the thermodynamic properties as the integrable limit is gradually approached. In the former limit the statistical mechanics of the system yields a phase diagram in the parameter space of
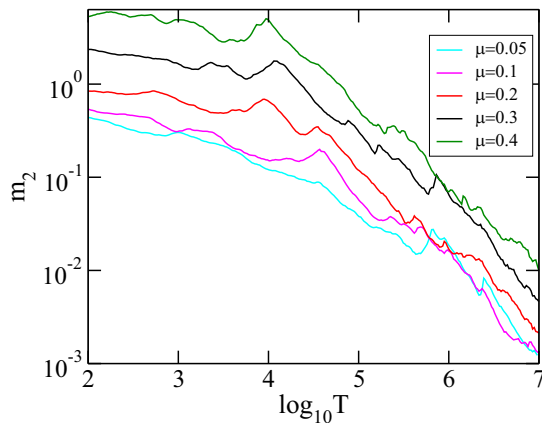

FIG. 7. The second moment [$m_2(T)$] of FTA distributions versus μ for $(a = 1.5, h = 5)$. The $\mu < \mu_c$ (≈ 0.17) case represents the non-Gibbs regime.
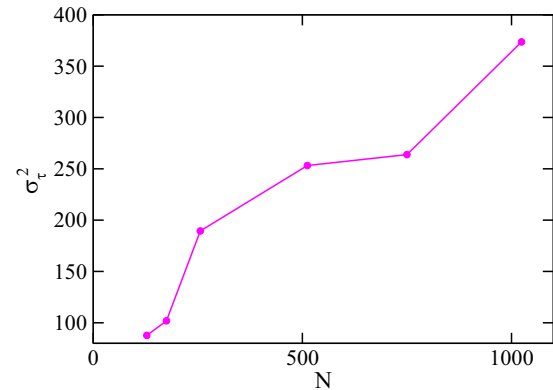

FIG. 8. The variance σ_τ^2 for $\mu = 0.05$ and $(a = 1.5, h = 5)$ as a function of system size N. This case corresponds to the non-Gibbs regime. The total integration time $T = 10^7$. The results are averaged over 5 different initial conditions.
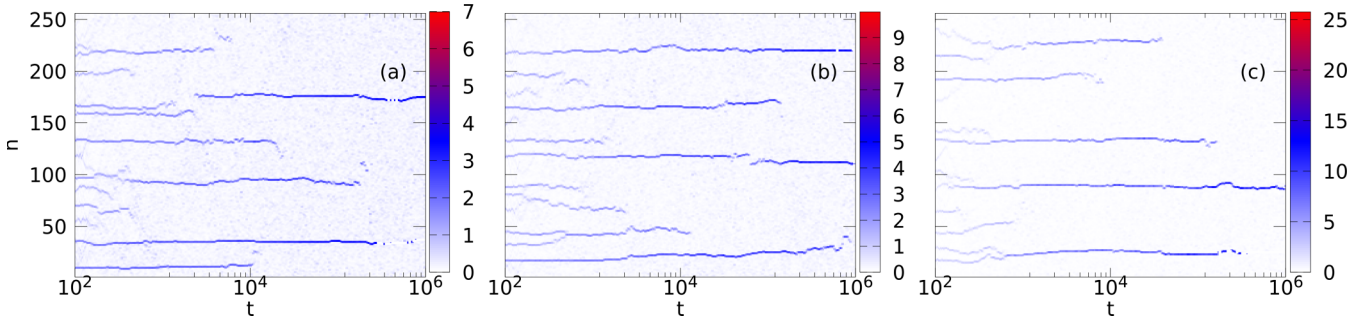
FIG. 9. The amplitude profiles in the non-Gibbs regime for (a) $\mu = 0.05$, (b) $\mu = 0.2$, and (c) $\mu = 0.5$ at $a = 0.2$, $h = 0.4$ for $N = 256$.

energy and norm densities. An infinite-temperature line decomposes the phase space into Gibbs and non-Gibbs regimes. The freedom afforded by the Salerno model is that we can achieve a transition from a non-Gibbs to a Gibbs regime for the same norm and energy parameters, upon variation of the strength of the nonlinear dispersive term (μ) interpolating between the two limits. Our analysis has shown that in the Gibbs regime, the SM is ergodic, and that as μ is increased toward the integrable limit, the region of the two-parameter space that thermalizes progressively expands. Nevertheless, there are some additional important features. Specifically, in the non-Gibbs regime, the ergodic properties heavily depend on the initial conditions and the ratio $h/h_{\beta=0}$. Additionally, the finite system size plays a crucial role and the TIO predictions are (expected to be) genuinely valid in the thermodynamic limit.

We believe that the present work provides insights into the thermalization of lattice systems and especially as we start approaching the integrable limit, including the role of parameters such as the lattice size and how "deep" in the non-Gibbs regime the initial conditions are. However, our results also raise a number of significant questions for future studies. Specifically, it is important to understand to what degree we can extend the present picture further toward the integrable limit and what happens in its immediate vicinity. Here, an important issue that arises is that additional conservation laws come into play [36]; how are these manifested in thermodynamic considerations? Their role in modifying (or dynamically constraining) the picture is something that is especially relevant to understand, in the immediate vicinity of the integrable limit and then further away from it. In that vein, revisiting also related studies exploring the creation and disappearance, as well as mobility, of discrete breathers as they interact with the phonon bath [45] (and how these mechanisms change while approaching integrability) would be an interesting direction. Additionally, while we have illustrated the relevance of finite size and of ratios such as $h/h_{\beta=0}$, obtaining a quantitative characterization of their role and of, e.g., the scaling dependence on the coherent structure (average) lifetime on them emerges as an especially relevant problem. This would greatly help in appreciating the influence of quasiergodicity ideas such as those put forth in [13,20]. Lastly, all of the above features have been explored in one-dimensional contexts yet it would be rather natural to extend considerations to higher-dimensional ones. These topics are presently under consideration and findings will be presented in future publications.

APPENDIX A: THE GRAND-CANONICAL APPROACH AND THE NONINTEGRABLE SM

1. $\beta \to \infty$ line

To obtain the $\beta \to \infty$ line we substitute the plane-wave like solution $\psi_n = \sqrt{d}e^{in\theta}$ with $\theta = \pi$ into Eq. (3) and obtain

$$h = -\frac{\gamma}{\mu^2}\ln(1 + \mu d) + \frac{\gamma}{\mu}d - 2d = -\frac{\gamma}{\mu}a + \frac{\gamma}{\mu^2}(e^{\mu a} - 1)$$

$$-\frac{2}{\mu}(e^{\mu a} - 1), \quad \text{and}$$

$$a = \frac{1}{\mu}\ln(1 + \mu d). \tag{A1}$$

2. $\beta = 0$ line

The grand-canonical partition function for the Hamiltonian Eq. (3) can be written in the form

$$Z = \int_0^\infty \int_0^{2\pi} \prod_{n=1}^N d\phi_n dA_n e^{-\beta(\mathcal{H} + \alpha\mathcal{A})}, \tag{A2}$$

where parameter α plays the role of chemical potential. Here a and h can be defined as

$$a = \frac{\langle\mathcal{A}\rangle}{N} = -\frac{1}{\beta N}\frac{\partial \ln(Z)}{\partial\alpha},$$

and

$$h = -\frac{1}{N}\frac{\partial \ln(Z)}{\partial \beta} - \alpha a.$$

After integration over the phase variable ϕ_m [see Eq. (6)] the following expression is obtained:

$$Z = (2\pi)^N \int_0^\infty \prod_{n=1}^N dA_n$$

$$\times I_0(2\beta\sqrt{A_nA_{n+1}})\, e^{-\beta \sum_n [(-\frac{\gamma}{\mu^2}+\frac{\alpha}{\mu})\ln|1+\mu A_n|+\frac{\gamma}{\mu}A_n]}. \quad (A3)$$

From this expression we find in the limit $\mu = 0$ (no non-local nonlinearity) the whole set of equations derived for the DNLS model with only local nonlinearity [25,45].

The line $\beta = 0$ which separates the Gibbsian from the non-Gibbsian regime for the Salerno lattice can be obtained in two ways:

a. Method I: Analytical

In the limit $\beta \to 0$, $I_0(2\beta\sqrt{A_mA_{m+1}}) \approx 1$. Now we take $\beta\gamma = x$ and $\beta\alpha = y$, $A = z$. Then Eq. (A3) can be expressed as

$$Z = (2\pi)^N E(x, y)^N, \quad (A4)$$

where

$$E(x, y) = \int_0^\infty dz\, e^{x\frac{1}{\mu^2}(\ln|1+\mu z|-\mu z)-y\frac{1}{\mu}\ln|1+\mu z|}. \quad (A5)$$

Here we take $y = \beta\alpha \equiv \delta$, a finite quantity. Consequently

$$a = -\left.\frac{\partial \ln E(0, y)}{\partial y}\right|_{y=\delta},$$

$$h + \alpha a = -\gamma\left.\frac{\partial \ln E(x, \delta)}{\partial x}\right|_{x=0} - \alpha\left.\frac{\partial \ln E(0, y)}{\partial y}\right|_{y=\delta}. \quad (A6)$$

We then obtain

$$a = -\frac{1}{E(0, y)}\left.\frac{\partial E(0, y)}{\partial y}\right|_{y=\delta} = \frac{1}{\delta - \mu},$$

$$h + \alpha a = -\gamma\frac{1}{E(0, \delta)}\left.\frac{\partial E(x, \delta)}{\partial x}\right|_{x=0} - \alpha\frac{1}{E(0, y)}\left.\frac{\partial E(0, y)}{\partial y}\right|_{y=\delta}$$

$$= \gamma\frac{1}{(\delta - 2\mu)(\delta - \mu)} + \alpha a,$$

$$h = \gamma\frac{a}{\left(\frac{1}{a} - \mu\right)}. \quad (A7)$$

We rewrite it as

$$h = \gamma\frac{a^2}{(1 - a\mu)}. \quad (A8)$$

b. Method II: Transfer integral operator (TIO) method

We apply the TIO method to Eq. (A3) which we rewrite as

$$Z = (2\pi)^N \int_0^\infty \prod_{m=1}^N dA_m I_0(2\beta\sqrt{A_mA_{m+1}})$$

$$\times e^{-\beta \sum_m[\frac{-\gamma+\alpha\mu}{2\mu^2}(\ln|1+\mu A_m|+\ln|1+\mu A_{m+1}|)+\frac{\gamma}{2\mu}(A_m+A_{m+1})]}. \quad (A9)$$
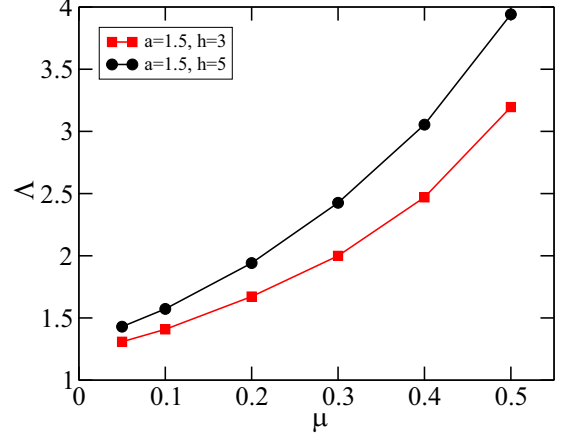

FIG. 10. The mLCE (Λ) for ($a = 1.5$, $h = 3$) (red squares) and ($a = 1.5$, $h = 5$) (black filled circles) as a function of μ for $N = 256$. In both cases the value of Λ increases with μ. See Fig. 11 for the finite time mLCE $\lambda(t)$.

In order to evaluate the integral, we consider the thermodynamic limit $N \to \infty$ of the system and evaluate using the integral equation

$$\int_0^\infty \prod_{m=1}^N dA_m K(A_m, A_{m+1})y(A_m) = \lambda y(A_{m+1}), \quad (A10)$$

where $K(x, y) = I_0(2\beta\sqrt{xy})e^{-\beta[\frac{-\gamma+\alpha\mu}{2\mu^2}(\ln|1+\mu x|+\ln|1+\mu y|)+\frac{\gamma}{2\mu}(x+y)]}$ is the kernel of the integral operator of Eq. (A10). Here $K(x, z)$ is symmetric and in the limit $z \to \infty$, $\iint K(x, z)dx\,dz$ should converge.

In the TIO, the partition function can be expressed in a simple form: $Z \approx (2\pi\lambda_0)^N$, where the largest eigenvalue (λ_0) of the kernel function is only taken into account. Therefore,
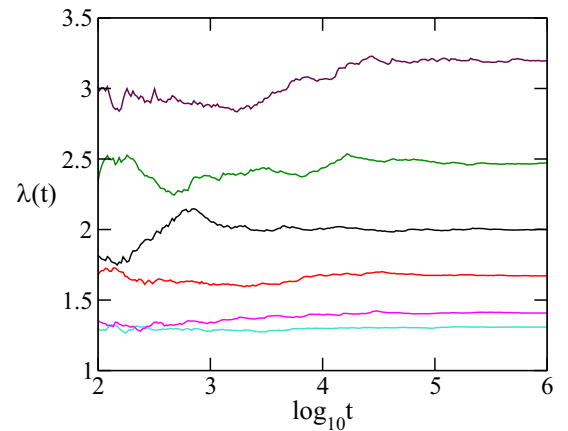

FIG. 11. The finite-time mLCE $\lambda(t)$ for different μ values ($\mu = 0.05, 0.1, 0.2, 0.3, 0.4, 0.5$, from bottom to top) and for the parameters ($a = 1.5$, $h = 3$). The value of $\lambda(t)$ at $t = 10^6$ is shown in Fig. 10.

approximately the norm and energy densities are

$$a = -\frac{1}{\beta\lambda_0}\frac{\partial\lambda_0}{\partial\alpha}, \quad \text{and} \quad h = -\frac{1}{\lambda_0}\frac{\partial\lambda_0}{\partial\beta} - \alpha a. \quad (A11)$$

APPENDIX B: THE FINITE-TIME mLCE

As an additional diagnostic, we estimate the maximal Lyapunov characteristic exponent (mLCE) Λ [46–48], which is in general a measure of the degree of chaos in the system. More concretely, we derive the evolution equations for small perturbations $\chi_n(0)$ of the initially injected plane-wave profile $\psi_n(0)$ adopting the standard procedure based on the linearization in the presence of small perturbations and numerically solve the obtained variational equations

$$i\frac{d\chi_n}{dt} = (1 + \mu|\psi_n|^2)(\chi_{n+1} + \chi_{n-1}) + \mu(\psi_{n+1} + \psi_{n-1})$$
$$\times (\psi_n^*\chi_n + \psi_n\chi_n^*) + \gamma(2|\psi_n|^2\chi_n + \psi_n^2\chi_n^*). \quad (B1)$$

The mLCE is then obtained as

$$\Lambda = \lim_{t\to\infty}\lambda(t) = \lim_{t\to\infty}\frac{1}{t}\ln\frac{||\chi(t)||}{||\chi(0)||}, \quad (B2)$$

with $\lambda(t)$ denoting the so-called finite-time mLCE, $\chi(t) = (\chi_1, \chi_2, \ldots, \chi_N)$ being the deviation vector and $||\cdot||$ the usual Euclidean norm.

Figure 10 shows that the mLCE $\Lambda > 0$ for both the Gibbs and non-Gibbs regimes, which confirms the chaoticity of the system. Also, we find that the mLCE grows exponentially as a function of μ.

Figure 11 shows the finite-time mLCE $\lambda(t)$ for different μ values ($\mu = 0.05, 0.1, 0.2, 0.3, 0.4, 0.5$, from bottom to top) and for the parameters ($a = 1.5, h = 3$). It is clear that by $t = 10^6$ (actually even before that time) the finite-time mLCE has saturated to specific values. These values of $\lambda(t)$ at $t = 10^6$ are shown in Fig. 10.

[1] S. Aubry, A unified approach to the interpretation of displacive and order-disorder systems. I. Thermodynamical aspect, J. Chem. Phys. **62**, 3217 (1975).

[2] E. A. Jackson, Nonlinearity and irreversibility in lattice dynamics, Rocky Mt. J. Math. **8**, 127 (1978).

[3] J. Bouchaud, Weak ergodicity breaking and aging in disordered systems, J. Phys. I France **2**, 1705 (1992).

[4] L. Casetti, M. Cerruti-Sola, M. Pettini, and E. G. D. Cohen, The Fermi-Pasta-Ulam problem revisited: Stochasticity thresholds in nonlinear Hamiltonian systems, Phys. Rev. E **55**, 6566 (1997).

[5] C. Giardinà, R. Livi, A. Politi, and M. Vassalli, Finite Thermal Conductivity in 1D Lattices, Phys. Rev. Lett. **84**, 2144 (2000).

[6] M. Johansson and K. O. Rasmussen, Statistical mechanics of general discrete nonlinear Schrödinger models: Localization transition and its relevance for Klein-Gordon lattices, Phys. Rev. E **70**, 066610 (2004).

[7] G. Bel and E. Barkai, Weak ergodicity breaking with deterministic dynamics, Europhys. Lett. **74**, 15 (2006).

[8] S. Iubini, R. Franzosi, R. Livi, G.-L. Oppo, and A. Politi, Discrete breathers and negative-temperature states, New J. Phys. **15**, 023032 (2013).

[9] G. Biroli and M. Tarzia, Delocalized glassy dynamics and many-body localization, Phys. Rev. B **96**, 201114(R) (2017).

[10] P. Buonsante, R. Franzosi, and A. Smerzi, Phase transitions at high energy vindicate negative microcanonical temperature, Phys. Rev. E **95**, 052135 (2017).

[11] C. Danieli, D. K. Campbell, and S. Flach, Intermittent many-body dynamics at equilibrium, Phys. Rev. E **95**, 060202(R) (2017).

[12] M. Onorato, L. Vozella, D. Proment, and Y. V. Lvov, Route to thermalization in the α-Fermi–Pasta–Ulam system, Proc. Natl. Acad. Sci. U.S.A. **112**, 4208 (2015).

[13] T. Mithun, C. Danieli, Y. Kati, and S. Flach, Dynamical Glass and Ergodization Times in Classical Josephson Junction Chains, Phys. Rev. Lett. **122**, 054102 (2019).

[14] B. Rumpf, Simple statistical explanation for the localization of energy in nonlinear lattices with two conserved quantities, Phys. Rev. E **69**, 016618 (2004).

[15] A. Khare, K. Ø. Rasmussen, M. Salerno, M. R. Samuelsen, and A. Saxena, Discrete nonlinear Schrödinger equations with arbitrarily high-order nonlinearities, Phys. Rev. E **74**, 016607 (2006).

[16] B. Rumpf, Transition behavior of the discrete nonlinear Schrödinger equation, Phys. Rev. E **77**, 036606 (2008).

[17] M. Johansson, G. Kopidakis, and S. Aubry, KAM tori in 1D random discrete nonlinear Schrödinger model? Europhys. Lett. **91**, 50001 (2010).

[18] M. R. Samuelsen, A. Khare, A. Saxena, and K. O. Rasmussen, Statistical mechanics of a discrete Schrödinger equation with saturable nonlinearity, Phys. Rev. E **87**, 044901 (2013).

[19] O. Tieleman, C. Skokos, and A. Lazarides, Chaoticity without thermalisation in disordered lattices, Europhys. Lett. **105**, 20001 (2014).

[20] T. Mithun, Y. Kati, C. Danieli, and S. Flach, Weakly Nonergodic Dynamics in the Gross-Pitaevskii Lattice, Phys. Rev. Lett. **120**, 184101 (2018).

[21] V. N. Likhachev, T. Y. Astakhova, and G. A. Vinogradov, Thermodynamics and ergodicity of finite one-dimensional Toda and Morse lattices, Phys. Lett. A **354**, 264 (2006).

[22] S. Flach and C. Willis, Discrete breathers, Phys. Rep. **295**, 181 (1998).

[23] L. Pistone, S. Chibbaro, M. Bustamante, Y. L'vov, and M. Onorato, Universal route to thermalization in weakly-nonlinear one-dimensional chains, Math. Eng. **1**, 672 (2019).

[24] M. Salerno, Quantum deformations of the discrete nonlinear Schrödinger equation, Phys. Rev. A **46**, 6856 (1992).

[25] K. Ø. Rasmussen, T. Cretegny, P. G. Kevrekidis, and N. Grønbech-Jensen, Statistical Mechanics of a Discrete Nonlinear System, Phys. Rev. Lett. **84**, 3740 (2000).

[26] P. G. Kevrekidis, *The Discrete Nonlinear Schrödinger Equation* (Springer Science & Business Media, 2009).

[27] G. Gradenigo, S. Iubini, R. Livi, and S. N. Majumdar, Localization in the discrete nonlinear Schrödinger equation: Ensembles inequivalence and negative temperatures, J. Stat. Mech: Theory Exp. (2021) 023201.

[28] A. Mallick, T. Mithun, and S. Flach, Quench dynamics in disordered two-dimensional Gross-Pitaevskii lattices, Phys. Rev. A **102**, 033301 (2020).

[29] S. Iubini, L. Chirondojan, G.-L. Oppo, A. Politi, and P. Politi, Dynamical Freezing of Relaxation to Equilibrium, Phys. Rev. Lett. **122**, 084102 (2019).

[30] B. A. Malomed, Nonlinearity and discreteness: Solitons in lattices, in *Emerging Frontiers in Nonlinear Science*, edited by P. G. Kevrekidis, J. Cuevas-Maraver, and A. Saxena, Nonlinear Systems and Complexity, Vol. 32 (Springer, 2020).

[31] M. Ablowitz and J. Ladik, Nonlinear differential-difference equations and Fourier analysis, J. Math. Phys. **17**, 1011 (1976).

[32] M. Salerno, Discrete model for DNA-promoter dynamics, Phys. Rev. A **44**, 5292 (1991).

[33] T. R. Melvin, A. R. Champneys, and D. E. Pelinovsky, Discrete traveling solitons in the Salerno model, SIAM J. Appl. Dyn. Syst. **8**, 689 (2009).

[34] J. Gomez-Gardeñes, B. A. Malomed, L. M. Floría, and A. R. Bishop, Solitons in the Salerno model with competing nonlinearities, Phys. Rev. E **73**, 036608 (2006).

[35] Y. S. Kivshar and M. Salerno, Modulational instabilities in the discrete deformable nonlinear Schrödinger equation, Phys. Rev. E **49**, 3543 (1994).

[36] A. C. Cassidy, D. Mason, V. Dunjko, and M. Olshanii, Threshold for Chaos and Thermalization in the One-Dimensional Mean-Field Bose-Hubbard Model, Phys. Rev. Lett. **102**, 025302 (2009).

[37] D. Cai, A. R. Bishop, N. Grønbech-Jensen, and B. A. Malomed, Moving solitons in the damped Ablowitz-Ladik model driven by a standing wave, Phys. Rev. E **50**, R694(R) (1994).

[38] D. Cai, A. R. Bishop, and N. Grønbech-Jensen, Localized States in Discrete Nonlinear Schrödinger Equations, Phys. Rev. Lett. **72**, 591 (1994).

[39] S. Iubini, S. Lepri, and A. Politi, Nonequilibrium discrete nonlinear Schrödinger equation, Phys. Rev. E **86**, 011108 (2012).

[40] C. Danieli, T. Mithun, Y. Kati, D. K. Campbell, and S. Flach, Dynamical glass in weakly nonintegrable Klein-Gordon chains, Phys. Rev. E **100**, 032217 (2019).

[41] Freely available from http://www.unige.ch/~hairer/software.html.

[42] E. Hairer, S. P. Nørsett, and G. Wanner, *Solving Ordinary Differential Equations. I. Nonstiff Problems*, 2nd ed., Springer Series in Computational Mathematics, Vol. 14 (Springer, Berlin, 1993).

[43] C. Danieli, B. M. Manda, T. Mithun, and C. Skokos, Computational efficiency of numerical integration methods for the tangent dynamics of many-body Hamiltonian systems in one and two spatial dimensions, Math. Eng. **1**, 447 (2019).

[44] M. Peyrard, Nonlinear dynamics and statistical physics of DNA, Nonlinearity **17**, R1 (2004).

[45] K. Ø. Rasmussen, S. Aubry, A. Bishop, and G. Tsironis, Discrete nonlinear Schrödinger breathers in a phonon bath, Eur. Phys. J. B **15**, 169 (2000).

[46] G. Benettin, L. Galgani, A. Giorgilli, and J.-M. Strelcyn, Lyapunov characteristic exponents for smooth dynamical systems and for Hamiltonian systems: A method for computing all of them. Part 1: Theory, Meccanica **15**, 9 (1980).

[47] G. Benettin, L. Galgani, A. Giorgilli, and J. Strelcyn, Lyapunov characteristic exponents for smooth dynamical systems: A method for computing all of them. Part 2: Numerical application, Meccanica **15**, 21 (1980).

[48] C. Skokos, The Lyapunov characteristic exponents and their computation, in *Dynamics of Small Solar System Bodies and Exoplanets*, edited by J. J. Souchay and R. Dvorak (Springer, Berlin, 2010), pp. 63–135.